Online Material

OM1. Comparison of the detectability of minerals and organic compounds by different analytical techniques. Yes = detectable No = not detectable. na = not applicable.

Minerals	VNIR	XRD	Raman	LD-FTMS	SEM/EDS
Jarosite	yes	yes	yes	yes	yes
Alunite	yes	yes	yes	no	yes
Al-bearing silicate	yes	yes	yes	yes	yes
Tschermigite	yes	yes	no	no	no
Organic matter					
Detected	yes	no	yes	yes	no
Identifiable compound or chemistry	no	na	no	yes and no	no

OM2. Additional Site Description

The study site comprised the acid-sulfate area of Washburn Hot Springs. The acid-sulfate area was located on a steep slope above another area that also had several hot springs. The acid-sulfate area had "extensive diffuse gas seeps and an unknown number of fumaroles." (http://www.rcn.montana.edu/, accessed 6/26/19). Few studies have been conducted at WHS. Fournier (1989) analyzed two hot springs near the base of the WHS thermal area, both of which had higher pH (6.2) than the water analyzed herein (3.64 - 4.55) and concluded that the ammonia is likely responsible for the higher pH and "probably derived from distillation of buried sediments". Spear et al. (2005) found similar pH values in springs at the base of the WHS thermal area. They reported phylogenetic results of the microbes present in these higher pH springs. We sampled in the topographically higher, acid-sulfate area of WHS and consequently the microbial community would be expected to be different in Spear et al.'s (2005) study from that of the lower pH system studied here. Indeed, Henneberger (2008) characterized the microbial community of the acid-sulfate portion of WHS by epifluorescence microscopy and 16S rRNA. Henneberger's results show the presence of phylotypes (i) related to moderately thermophilic acidophilic archaea and (ii) related to uncultured or undescribed bacteria. These results are similar to those reported by Burns et al. (2009) for White Island, NZ and Mt. Hood, OR, USA. The acidophilic eukaryote *Cyanidium caldarium* was also observed.

OM3. Laser Desorption and Fourier-Transform Ion-Cyclotron Resonance Mass Spectrometry Principles

Laser Desorption and Ionization (LDI): Geological materials desorb and ionize associated organic matter in a manner similar to the matrix material in matrix-assisted laser desorption ionization (MALDI). Yan et al., (2007a) refer to this method as geomatrix-assisted laser desorption ionization (GALDI). We have used this technique on a number of substrates to establish detection limits, mineral spectra, spatial resolution, and correlated biological/geological maps at the micron scale (Scott et al., 2006; Richardson et al., 2008; Kotler et al., 2008; Yan et al., 2006, 2007a, b). More recently, Wörmer et al. (2014) used a similar method to measure lipid ratios in a marine-sediment core to determine sea surface temperature over time. They compared MALDI on geological samples with direct laser desorption ionization (LDI) without a matrix (i.e. GALDI). They found that the addition of a matrix only slightly improved the intensity in one sample. In our work and in Wörmer's et al. work, we observe that the addition of a matrix is not necessary for sample introduction and no additional sample preparation (heating, powdering, dissolving) is required, which would be a benefit is deployed on Mars or used for analysis of precious returned samples.

Introduction or interrogation of samples with lasers is not new. In fact, Laser-Induced Breakdown Spectroscopy (LIBS) is currently included in the ChemCam package on Mars Science Laboratory Rover (e.g., Lefebvre et al., 2016; Maurice et al., 2016)). LIBS also does not require sample preparation. While no sample preparation is required, all laser desorption methods due consume miniscule amounts of material. Further, LD-FTMS is a rapid way to explore laser desorption/ionization for different mineral matrices (Kotler et al., 2008; Richardson et al., 2008; Yan et al., 2007a,b; Scott et al., 2006). The results of such

experiments would provide insight into expectations for the Mars Organic Mass Analyzer Laser Desorption Instrument (MOMA-LDI) scheduled for the ExoMars mission (Goetz et al., 2016). This instrument has a different type of mass analyzer than the LD-FTMS in this study, but both employ laser desorption to introduce the sample to the instrument. Consequently, organic matter detection by LD-FTMS provides insight for interpretation of data collected by MOMA-LDI.

Fourier Transform Ion-Cyclotron Resonance (FT-ICR): The FT-ICR analytical technique consumes very tiny amounts of a sample because it had excellent detection limits. FT-ICR combines the mass analyzer and detector in the same space and thus differs from other types of mass spectrometers, which have a separate mass analyzer and detector. The other key difference is that the actual detection of the ions is non-destructive; thus, they can be stored, remeasured, and/or manipulated in multiple mass spectrometry steps (MS^n). The choice of mass spectrometer parameters depends on the type of experiment to be performed (see references in main paper for theory and applications of FT-ICR). The scanning or imaging LD-FT-ICR mass spectrometer used here was setup to survey the samples with in the mass-to-charge ratio (m/z) range up to 1000 amu with "high mass accuracy (error ± 0.003 amu), high resolution (typically >10,000), high sensitivity (~200 ions for peaks with S/N ~3), and high spatial resolution (~6 μm)" (Yan et al., 2006).

The chemical imaging LD-FTMS in this study integrates commercial Fourier transform mass spectrometry software with custom software for automated data acquisition and interpretation capable of generating maps based on chemical composition in 1.5 mm x 1.5 mm areas (Scott et al., 2006; Scott et al., 2003; Scott and Tremblay, 2002; Yan et al., 2006; McJunkin et al., 2002). The center-to-center distance was set to 100 microns for a closest packed pattern, resulting in an approximate 15 x 15 point grid. The resulting spectra report the m/z, which is the observed mass as detected by the mass spectrometer in ratio to the charge of the detected ion. The charge on all ions generated in the LD-FTMS is ± 1; no ions of higher positive or negative charge are generated.

Unlike current commercial LD-FTMS instruments that use an external source FTMS for ion desorption and ionization (Wörmer et al. 2014), the customized LD-FTMS used in this study was equipped with a traditional internal source; thus, the sample is inside the high magnetic field and all ions are desorbed directly into the FTMS cell. The internal source takes advantage of the magnetic field to hold the sample very steady (via Lenz's Law) for accurate laser positioning. Neutral species pass through the instrument cell undetected and consequently, this technique is not quantitative. The LD-FTMS was equipped with a 7T Oxford magnet (Oxford, England), a 355 nm Nd:YAG laser (Continuum, Santa Clara (CA)), an Odyssey control and data acquisition system (Finnigan FT/MS, Bremen, Germany), and laboratory designed automated software for data acquisition and interpretation (McJunkin et al. 2002, 2010; Yan et al., 2006). Sample handling procedures and FTMS parameters are described in detail elsewhere (Yan et al., 2007a,b; Kotler et al., 2008). Baseline-corrected, zero-filled (data processing technique to improve digital resolution) raw data were analyzed by Fourier transform to produce the mass spectra. A chemical image of the sample was generated using an automatic mapping function with very high reproducibility for location return. Composition assignments were made according to procedures

described previously (Kotler et al., 2008; Richardson et al. 2008). The samples were subjected to a vacuum (10^{-9} to 10^{-10} Torr) for a minimum of one hour prior to analysis to remove volatile surface contaminants. Previous studies of surface exchange reactions suggest that exposure to the vacuum has little or no effect on non-volatile organic compounds (Scott et al., 1997). This minimizes the potential for contamination from volatile organic compounds that may be introduced during sample handling.

Assignment of elemental compositions to individual or groups of m/z values: We refer the reader to articles that discuss the assignment of stoichiometries at line 240: "Composition assignments were made according to procedures described previously (Kotler et al., 2008; Richardson et al. 2008)." The clearest example is provided in the Kotler et al. (2008) paper.

Kotler et al. (2008) provides a detailed explanation for the assignment of compositions (stoichiometries). We note on line 247 that the instrumental error is ±0.003 and the resolving power is 10,000. Our focus was on surveying the samples for species with m/z less than 1000 amu and consequently, compositions are constrained to be within 0.003 amu of the exact mass of the most abundant isotope, e.g., mass of ^{1}H is 1.007825 based on ^{12}C mass of 12.000000. For this range (±0.003 amu), we can tell the difference between compositions to ±3 in the third decimal place. Table 4 of Kotler et al. (2008) illustrates our ability to distinguish among different compositions. In this table, the nominal mass is listed as column headers. The exact masses for the corresponding nominal mass are listed in the columns for each theoretical structure. If the observed isotope mass is compared with the calculated masses of each theoretical structure in the rows below and the absolute difference from the observed mass is greater than 0.002 then that composition is eliminated; Kotler et al. (2008) used experimental parameters that reduced the error to ±0.002 amu. In Kotler et al. (2008) Table 4, the mass of the third theoretical composition matches the observed mass within the margin of error and this composition is assigned to be that of the third theoretical species.

OM4. Samples from Water Sources

Water samples were collected in acid-washed syringes and filtered through 0.2- µm nylon filters in the field. Samples for anion analysis were collected first. Samples for cation analysis were collected second and then preserved at pH < 2 with Ultrex® nitric acid (Mallinckrodt Baker 65 – 70 wt%) in the field. All water samples were refrigerated until analysis. Water samples were analyzed for anion concentrations by ion chromatography (Dionex DX-500 IC) at the University of Montana Environmental Biogeochemistry Laboratory. Unfortunately, concentrations of SO_4^{2-}, which were consistent with S concentrations reported by ICP, were too high to allow quantification of other anions.

OM5. Table of chemical and physical properties of WHS water samples. bdl = below detection limit.

ANALYTE	DETECTION LIMIT	UNITS				
Site Name			Blank	WWS8	WWS5	WWS5 (duplicate)
T		°C		44	78	
pH				4.55	3.64	
Elevation		m		2,526	5,477	
UTM				545089	545103	
UTM				4957184	4956978	
SO_4^{2-}		g/L	bdl	2.80	2.70	2.70
B	10	µg/L	bdl	15,500	11,300	10,900
Li	10	µg/L	bdl	bdl	40	40
S	50	µg/L	bdl	897,160	946,430	923,590
Ag	1	µg/L	bdl	bdl	bdl	bdl
Al	50	µg/L	bdl	890	1,440	1,300
As	30	µg/L	bdl	bdl	bdl	bdl
Ba	10	µg/L	bdl	70	60	150
Be	5	µg/L	bdl	bdl	bdl	bdl
Bi	50	µg/L	bdl	bdl	bdl	bdl
Ca	50	µg/L	bdl	12,600	48,300	46,100
Cd	10	µg/L	bdl	bdl	bdl	bdl
Co	10	µg/L	bdl	bdl	bdl	bdl
Cr	10	µg/L	bdl	bdl	bdl	bdl
Cu	5	µg/L	bdl	bdl	bdl	bdl
Fe	50	µg/L	bdl	2,170	1,440	1,360
K	100	µg/L	bdl	7,700	27,000	25,900
La	10	µg/L	bdl	bdl	20	20
Mg	50	µg/L	bdl	6,610	22,000	21,300
Mn	5	µg/L	bdl	196	722	697
Mo	10	µg/L	bdl	bdl	bdl	bdl
Na	50	µg/L	260	12,000	52,100	48,200
Ni	10	µg/L	bdl	bdl	bdl	bdl
P	50	µg/L	bdl	bdl	bdl	bdl
Pb	30	µg/L	bdl	bdl	bdl	bdl
Sb	50	µg/L	bdl	bdl	bdl	bdl
Sc	1	µg/L	bdl	bdl	bdl	bdl
Si	100	µg/L	bdl	113,404	137,104	136,104
Sn	50	µg/L	bdl	bdl	bdl	bdl
Sr	1	µg/L	bdl	152	185	184
Ti	10	µg/L	bdl	bdl	bdl	bdl
V	10	µg/L	bdl	10	bdl	bdl
W	50	µg/L	bdl	bdl	bdl	bdl
Y	5	µg/L	bdl	bdl	116	115
Zn	5	µg/L	19	139	1,150	924
Zr	10	µg/L	bdl	bdl	bdl	bdl

OM6. Major and minor element chemistry of samples from three thermal sites and background site (W3). D.L = detection limit. C+IR= combustion followed by infrared spectrometry. dup = duplicate analysis. LOI = loss on ignition.

ANALYTE	METHOD	D.L.	UNITS	W1	W1-dup	W2	W3	W4
C	C+IR	0.01	%	1.28	1.29	0.69	14.1	1.19
S	C+IR	0.01	%	0.73	0.77	1.85	0.31	1.05
SiO_2	XRF	0.01	%	85.5	85.4	87	55.2	82.2
Al_2O_3	XRF	0.01	%	0.52	0.52	0.81	9.06	0.39
CaO	XRF	0.01	%	0.03	0.03	0.06	0.37	0.02
MgO	XRF	0.03	%	0.22	0.22	0.21	0.43	0.3
Na_2O	XRF	0.02	%	0.08	0.07	0.1	0.63	0.1
K_2O	XRF	0.01	%	0.06	0.06	0.09	2.99	0.06
Fe_2O_3	XRF	0.01	%	0.57	0.57	0.32	2	0.95
MnO	XRF	0.01	%	<0.01	<0.01	<0.01	0.02	<0.01
TiO_2	XRF	0.01	%	3.49	3.48	1.8	0.38	7.72
P_2O_5	XRF	0.01	%	0.02	0.02	<0.01	0.09	0.02
Cr_2O_3	XRF	0.01	%	0.02	0.02	0.04	0.03	0.09
Rb	XRF	2	PPM	2	<2	<2	113	5
Sr	XRF	2	PPM	80	78	277	98	82
Y	XRF	2	PPM	<2	<2	<2	60	<2
Zr	XRF	2	PPM	633	633	327	309	1230
Nb	XRF	2	PPM	22	22	12	28	56
Ba	XRF	20	PPM	>4000	>4000	>4000	930	>4000
LOI	XRF	0.01	%	4.15	4.05	5	27.4	5.95
Sum	XRF	0.01	%	95.3	95	96	98.8	99.5
Al	ICP	0.01	%	0.28	0.29	0.4	4.03	0.21
Ba	ICP	5	PPM	3450	3530	1800	675	6490
Ca	ICP	0.01	%	0.03	0.02	0.01	0.2	0.03
Cr	ICP	1	PPM	168	177	284	210	573
Cu	ICP	0.5	PPM	112	117	4.4	11.1	4
Fe	ICP	0.01	%	0.39	0.42	0.2	1.27	0.65
K	ICP	0.01	%	0.05	0.05	0.07	2.02	0.04
Li	ICP	1	PPM	6	6	9	17	6
Mg	ICP	0.01	%	<0.01	<0.01	0.01	0.16	0.01
Mn	ICP	5	PPM	16	18	19	139	68
Na	ICP	0.01	%	0.03	0.03	0.04	0.37	0.04
Ni	ICP	0.5	PPM	13.4	16	15.7	14.3	21.1
P	ICP	50	PPM	80	90	<50	330	70
S	ICP	0.01	%	0.7	0.84	1.49	0.36	1.03
Sr	ICP	0.5	PPM	67.5	69.7	188	82.9	72.2
Ti	ICP	0.01	%	1.78	1.84	0.9	0.16	3.38
V	ICP	1	PPM	38	39	20	22	50
Zn	ICP	1	PPM	2	2	2	26	2
Zr	ICP	0.5	PPM	90.6	87.4	130	110	181

OM6, continued.

ANALYTE	METHOD	D.L.	UNITS	W1	DUP-W1	W2	W3	W4
Ag	ICPMS	0.02	PPM	0.33	0.31	0.23	0.14	0.04
As	ICPMS	1	PPM	2	<1	<1	9	<1
Be	ICPMS	0.1	PPM	<0.1	<0.1	<0.1	1.9	<0.1
Bi	ICPMS	0.04	PPM	0.29	0.32	0.06	0.32	0.32
Cd	ICPMS	0.02	PPM	<0.02	<0.02	<0.02	0.11	<0.02
Ce	ICPMS	0.05	PPM	4.49	4.9	8.36	65.2	4.79
Co	ICPMS	0.1	PPM	5.6	5.5	1.9	2.8	0.6
Cs	ICPMS	0.05	PPM	0.18	0.1	0.19	2.3	0.17
Ga	ICPMS	0.1	PPM	4.3	4.3	2.3	13	5.2
Ge	ICPMS	0.1	PPM	<0.1	<0.1	<0.1	<0.1	0.1
Hf	ICPMS	0.02	PPM	3.52	3.58	2.97	3.32	5.35
In	ICPMS	0.02	PPM	<0.02	<0.02	<0.02	0.06	<0.02
La	ICPMS	0.1	PPM	4.4	4.7	9.8	34.5	8.4
Lu	ICPMS	0.01	PPM	0.03	0.03	0.05	0.34	0.06
Mo	ICPMS	0.05	PPM	3.88	4.1	2.18	3.86	4.76
Nb	ICPMS	0.1	PPM	23	23.4	11.7	30.8	50.7
Pb	ICPMS	0.5	PPM	24.9	25.5	47	28.5	41.8
Rb	ICPMS	0.2	PPM	0.9	1	1.9	86.2	1.7
Sb	ICPMS	0.05	PPM	0.87	0.89	2.3	1.01	1.63
Sc	ICPMS	0.1	PPM	1.8	1.7	2.1	5.2	1.3
Se	ICPMS	2	PPM	3	3	<2	<2	<2
Sn	ICPMS	0.3	PPM	3.9	4.1	3.4	4.2	8.6
Ta	ICPMS	0.05	PPM	1.76	1.92	0.82	2.37	3.83
Tb	ICPMS	0.05	PPM	<0.05	<0.05	<0.05	0.82	<0.05
Te	ICPMS	0.05	PPM	0.78	0.71	0.06	0.08	0.33
Th	ICPMS	0.2	PPM	1.1	1.2	1.7	12.7	2
Tl	ICPMS	0.02	PPM	0.06	0.07	0.03	0.53	0.02
U	ICPMS	0.1	PPM	0.7	0.8	0.6	2.6	1.3
W	ICPMS	0.1	PPM	1.8	1.6	0.9	1.4	2.2
Y	ICPMS	0.1	PPM	0.8	0.7	1.6	24.8	1.9
Yb	ICPMS	0.1	PPM	0.1	0.1	0.3	2.4	0.3

OM7. Table 3. X-ray diffraction data for samples from WHS.

Reference mineral diffraction peaks	Sample diffraction peaks					
	W2		WS8		WS5	
	°2 θ	d (Å)	°2 θ	d (Å)	°2 θ	d (Å)
Copiapite					4.91	18.33
Kaolinite, Copiapite					10.01	8.80
Clinoptilolite					10.46	8.45
Clinoptilolite			10.74	8.20		
Clinoptilolite					11.55	7.66
Tschermigite, Kaolinite					12.45	7.10
Clinoptilolite					13.99	6.32
Jarosite	14.91	5.94	14.89	5.94		
Alunite, Jarosite	15.54	5.70	15.42	5.74		
Copiapite					16.10	5.50
Tschermigite,					17.19	
Jarosite	17.43	5.08	17.41	5.08		
Tschermigite, Clinoptilolite					17.66	5.03
Alunite	17.91	4.95	17.72	4.99		
Tschermigite					20.42	4.34
Quartz	20.89	4.25	20.81	4.26	21.08	4.21
Tschermigite					21.67	4.10
Tschermigite					23.37	3.80
Clinoptilolite					23.46	3.78
Copiapite					24.01	3.70
Jarosite			24.43	3.63		
Alunite	25.50	3.48	25.40	3.50		
Quartz	26.67	3.34	26.57	3.35	26.59	3.36
Tschermigite					27.15	3.28
Jarosite	28.51	3.13	28.71	3.10		
Tschermigite, Copiapite					29.46	3.03
Jarosite			29.01	3.07		
Alunite	29.94	2.98	29.75	2.99		
Alunite, Jarosite			31.14	2.86		
Tschermigite					32.59	2.74
Jarosite	35.21	2.54	35.24	2.54		
Quartz	36.58	2.45				
Quartz, Alunite, Jarosite	39.44	2.28	39.37	2.28		
Tschermigite					39.47	2.29
Quartz	40.34	2.23				
Quartz	42.47	2.12				
Quartz, Jarosite	45.83	1.97	45.88	1.97		
Tschermigite					46.78	1.94
Silicon	47.33	1.91				
Alunite			47.60	1.90		
Jarosite, Quartz	50.17	1.816	50.01	1.82		
Alunite	52.33	1.74				
Silicon	56.15	1.63				
Quartz	59.98	1.54				
Alunite, Jarosite	61.71	1.50				
Quartz, Silicon	68.32	1.37				

OM8. LD-FTMS spectrum for site W2 showing (a) background jarosite mineral with Fe and K peaks and (b) possible fatty acid signature at m/z 315.253 with the assignment $C_{16}H_{38}NO_2K^+$.

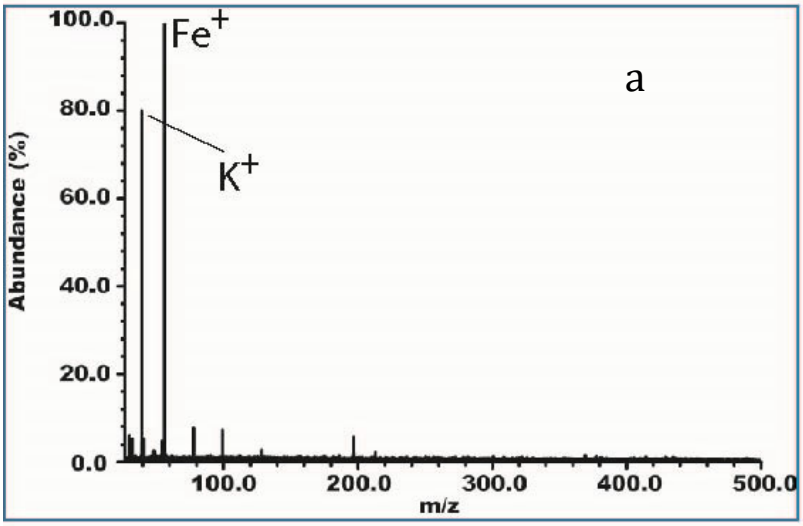

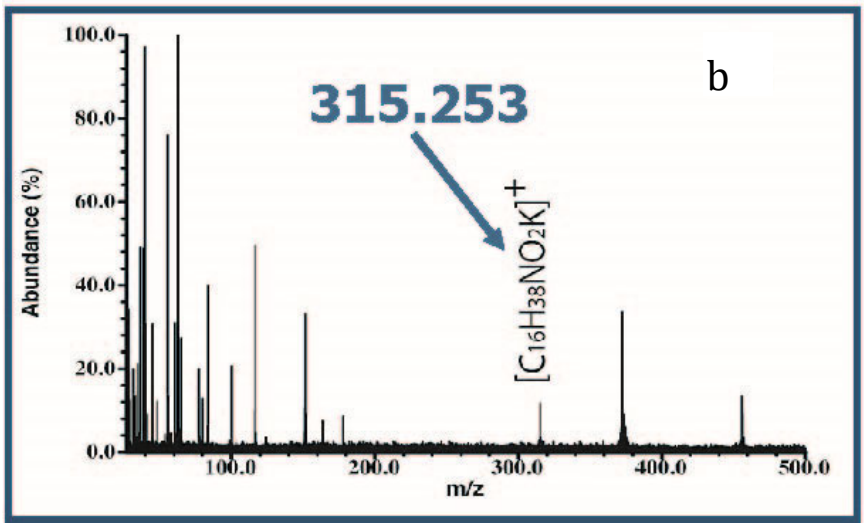

OM References

Burns, B.P., Anitori, R., Butterworth, P., Henneberger, R., Goh, F., Allen, M.A., Ibanez-Peral, R., Bergquist, P.L., Walter, M.R., and Neilan, B.A. (2009) Modern analogues and the

early history of microbial life. Precambrian Research, 173(1-4), 10-18.
Fournier, R.O. (1989) Geochemistry and dynamics of the Yellowstone-National-Park hydrothermal system. Annual Review of Earth and Planetary Sciences, 17, 13-53.
Goetz, W., Brinckerhoff, W.B., Arevalo, R., Freissinet, C., Getty, S., Glavin, D.P., Siljestrom, S., Buch, A., Stalport, F., Grubisic, A., Li, X., Pinnick, V., Danell, R., van Amerom, F.H.W., Goesmann, F., Steininger, H., Grand, N., Raulin, F., Szopa, C., Meierhenrich, U., Brucato, J.R., and Team, M.S. (2016) MOMA: the challenge to search for organics and biosignatures on Mars. International Journal of Astrobiology, 15(3), 239-250.
Henneberger, R.M. (2008) The microbial diversity and ecology of selected andesitic hydrothermal environments. Macquarie University, Australia.
Kotler, J.M., Hinman, N.W., Yan, B., Stoner, D.L., and Scott, J.R. (2008) Glycine identification in natural jarosites using laser desorption Fourier transform mass spectrometry: Implications for the search for life on Mars. Astrobiology, 8(2), 253-266.
Lefebvre, C., Catala-Espi, A., Sobron, P., Koujelev, A., and Leveille, R. (2016) Depth-resolved chemical mapping of rock coatings using Laser-Induced Breakdown Spectroscopy: Implications for geochemical investigations on Mars. Planetary and Space Science, 126, 24-33.
Maurice, S., Clegg, S.M., Wiens, R.C., Gasnault, O., Rapin, W., Forni, O., Cousin, A., Sautter, V., Mangold, N., Le Deit, L., Nachon, M., Anderson, R.B., Lanza, N.L., Fabre, C., Payre, V., Lasue, J., Meslin, P.Y., Leveille, R.J., Barraclough, L., Beck, P., Bender, S.C., Berger, G., Bridges, J.C., Bridges, N.T., Dromart, G., Dyar, M.D., Francis, R., Frydenvang, J., Gondet, B., Ehlmann, B.L., Herkenhoff, K.E., Johnson, J.R., Langevin, Y., Madsen, M.B., Melikechi, N., Lacour, J.L., Le Mouelic, S., Lewin, E., Newsom, H.E., Ollila, A.M., Pinet, P., Schroeder, S., Sirven, J.B., Tokar, R.L., Toplis, M.J., d'Uston, C., Vaniman, D.T., and Vasavada, A.R. (2016) ChemCam activities and discoveries during the nominal mission of the Mars Science Laboratory in Gale crater, Mars. Journal of Analytical Atomic Spectrometry, 31(4), 863-889.
McJunkin, T.R., and Scott, J.R. (2010) Application of Fuzzy logic for automated interpretation of mass spectra. In R.E. Vargas, Ed. Fuzzy Logic: Theory, Programming and Applications, p. 85–114. Nova Science Publishers, Hauppauge, NY.
McJunkin, T.R., Tremblay, P.L., and Scott, J.R. (2002) Automation and control of an imaging internal laser desorption Fourier transform mass spectrometer (I2LD-FTMS). JALA: Journal of the Association for Laboratory Automation, 7(3), 76-83.
Richardson, C.D., Hinman, N.W., McJunkin, T.R., Kotler, J.M., and Scott, J.R. (2008) Exploring Biosignatures Associated with Thenardite by Geomatrix-Assisted Laser Desorption/Ionization Fourier Transform Ion Cyclotron Resonance Mass Spectrometry (GALDI-FTICR-MS). Geomicrobiology Journal, 25(7-8), 432-440.
Scott, J.R., Baker, L.S., Everett, W.R., Wilkins, C.L., and Fritsch, I. (1997) Laser desorption Fourier transform mass spectrometry exchange studies of air-oxidized alkanethiol self-assembled monolayers on gold. Analytical Chemistry, 69(14), 2636-2639.
Scott, J.R., McJunkin, T.R., and Tremblay, P.L. (2003) Automated analysis of mass spectral data using fuzzy logic classification. JALA: Journal of the Association for Laboratory Automation, 8(2), 61-63.
Scott, J.R., and Tremblay, P.L. (2002) Highly reproducible laser beam scanning device for an internal source laser desorption microprobe Fourier transform mass spectrometer.

Review of Scientific Instruments, 73(3), 1108-1116.
Scott, J.R., Yan, B., and Stoner, D.L. (2006) Spatially-correlated mass spectrometric analysis of microbe–mineral interactions. Journal of Microbiological Methods, 67(2), 381-384.
Spear, J.R., Walker, J.J., McCollom, T.M., and Pace, N.R. (2005) Hydrogen and bioenergetics in the Yellowstone geothermal ecosystem. Proceedings of the National Academy of Sciences of the United States of America, 102(7), 2555-2560.
Wormer, L., Elvert, M., Fuchser, J., Lipp, J.S., Buttigieg, P.L., Zabel, M., and Hinrichs, K.U. (2014) Ultra-high-resolution paleoenvironmental records via direct laser-based analysis of lipid biomarkers in sediment core samples. Proceedings of the National Academy of Sciences of the United States of America, 111(44), 15669-15674.
Yan, B., McJunkin, T.R., Stoner, D.L., and Scott, J.R. (2006) Validation of fuzzy logic method for automated mass spectral classification for mineral imaging. Applied Surface Science, 253(4), 2011-2017.
Yan, B.Z., Stoner, D.L., Kotler, J.M., Hinman, N.W., and Scott, J.R. (2007a) Detection of biosignatures by geomatrix-assisted laser desorption/ionization (GALDI) mass spectrometry. Geomicrobiology Journal, 24(3-4), 379-385.
Yan, B.Z., Stoner, D.L., and Scott, J.R. (2007b) Direct LD-FTMS detection of mineral-associated PAHs and their influence on the detection of co-existing amino acids. Talanta, 72(2), 634-641.